

Assessment of OLED Head Mounted Display for vision research with Virtual Reality

Matteo Toscani

*Department of General Psychology
Justus-Liebig-Universität Gießen
Giessen, Germany*
matteo.toscani@psychol.uni-giessen.de

Giuseppe Claudio Guarnera

*Department of Computer Science
Norwegian University of Science and
Technology, University of York
Gjøvik, Norway; York, United Kingdom*
giuseppe.guarnera@ntnu.no

Raquel Gil

*Department of General Psychology
Justus-Liebig-Universität Gießen
Giessen, Germany*
Raquel.Gil-Rodriguez@psychol.uni-giessen.de

Assim Kalouaz

*Department of General Psychology
Justus-Liebig-Universität Gießen
Giessen, Germany*
assim.kalouaz@gmail.com

Dar'ya Guarnera

*Department of Computer Science
Norwegian University of Science and
Technology
Gjøvik, Norway*
darya.guarnera@ntnu.no

Karl R. Gegenfurtner

*Department of General Psychology
Justus-Liebig-Universität Gießen
Giessen, Germany*
karl.r.gegenfurtner@psychol.uni-giessen.de

Abstract— Vision researchers often rely on visual display technology to present observers with controlled stimuli, usually by means of a calibrated computer screen. Virtual Reality (VR) may allow a similar level of control, together with higher realism of the stimulation and a visual field larger than what is achievable on a standard computer monitor. To produce the desired luminance and color of the stimuli, accurate characterization of the spectral properties of the display is necessary. However, this process might not be trivial on VR displays, because 1) the Head Mounted Displays (HMD) used in VR are typically designed to be light-weight and low energy consuming, thus they might not meet some of the standard assumptions in display calibration, 2) the VR software might affect the color and luminance signal in a complex way, further complicating the calibration process. Here we show that 1) a common, off-the-shelf display used in our experiments behaves similarly to a standard OLED monitor, 2) the VR gaming engine we tested (Unreal Engine 4) introduces a complex behavior, 3) which can be disabled. This allows to accurately control colors and luminance emitted by the display, thus enabling its use for perceptual experiments.

I. INTRODUCTION

More than two decades ago, digital display became popular to render experimental stimuli for vision research (1). They allow to easily generate colorimetrically calibrated complex images, otherwise extremely difficult to produce with traditional image technologies, such as photography or printing (2). However, computer monitors offer a relatively small field of view, covering only part of the scene that the observer is facing. For instance, an Eizo CG223W LCD monitor, at the standard viewing distance of 57 cm, would present about 45 degrees of visual angle (dva) field of view on the horizontal dimension, whereas a HTC Vive Pro Eye HMD allows about 100 dva. Furthermore, in order to control the location of the retinal projections of the light emitted by a typical computer display (e.g. present a stimulus at a given eccentricity in the visual field), observers are often seated in front of a computer with their head stabilized by a chinrest or a bite bar, whereas the HMD, mounted on the observer's head, completely removes the need for stabilizing it.

In fact, with a HMD headset observers are completely immersed in the VR environment and free to move, while the

location of the images projected on their retinæ can be controlled. Furthermore, the dramatic developments in the VR technology over the last few years yield an almost photo-realistic rendering of the virtual scenes (3,4).

Realism of the stimuli is a crucial factor for vision research, at least concerning color vision. One prominent aspect of color vision is color constancy, the ability of the visual system to stably perceive the color of objects, when the color of the illumination changes. Without such an ability, color would not be informative about the surfaces' material, as it would depend on the illumination as well as on the reflectance spectrum. Color constancy increases with the level of complexity of the visual scene and can be quantified with an index from 0%, the perceived color of a surface as predicted by the change in the illumination, to 100%, the perceived color of a surface does not change with the illumination. This index ranges from 30% (5), in experiments with flat colored patches, to about 90% with realistic viewing conditions and stimuli (6,7). Presumably, this is because only realistic scenes include cues which are used by the visual system for discounting the contribution of the illumination.

Naturalism of experimental stimuli can be crucial in vision research behind color. In fact, there is evidence that the visual system uses the statistical regularities of real-world as diagnostic image features for surfaces' reflectance properties such as specularities (8). Although investigating vision with realistic stimulation may reveal perceptual mechanism which are not at work with simpler stimuli, the experimental conditions are difficult to control in the real world. Therefore, experiments tend to be more time-consuming and more prone to errors than with a computer monitor.

Because of the recent development in VR technology (3,4), VR offers an ideal tool for maximizing realism and control of the experimental stimuli. VR has become increasingly used in psychology (e.g., 9-11) and neuropsychology (12). However, its use is surprisingly limited (see 13) in visual perception in general, and color vision in particular, where a fine control of the light emitted by the HMD is needed. This might be partly explained by the difficulty in calibrating the display. Indeed, the HMD is designed to be light-weight and low energy consuming (14),

thus it might not meet the standard assumptions for the display calibration (15,16), and the VR software used for the rendering

In this work, we measured the spectral properties of a HTC Vive Pro Eye HMD, controlled by Psychtoolbox 3 (17) via MATLAB, and by Unreal Engine 4 (18), with and without the post-processing routines. We used our measures to perform a standard calibration procedure which is meant to allow controlling the color of the light emitted by the display. When controlled via Psychtoolbox, the HMD behaves as a computer monitor, and therefore a standard calibration allows controlling the produced colors. With the Unreal Engine we could achieve a satisfactory result only when the post-processing routines were disabled.

II. METHODS

We characterized the HMD with the series of measures necessary for a standard color calibration procedure (15,16). We measured the spectrum of the emitted light from the center of the display. The headset was placed on a flat surface, while a tele-spectrometer was held by a tripod, such that its optical axis was orthogonal to the center of the HMD screen. When the HMD was controlled via Psychtoolbox, we measured different intensities corresponding to 20 linearly sampled bit values. We did this for the three channels (R,G and B) individually, as well as for the three channels together, by assigning the same bit value to all channels simultaneously.

When using Unreal Engine 4, we could not directly control the displayed intensity. Instead, we changed the reflectance parameters of a perfectly lambertian surface included in a virtual scene, specifically designed for the calibration purpose. By changing the reflectance, we could not directly control the absolute luminance, which depends also on the intensity of the illumination. In order to isolate the activity of the R,G,B channels while changing the reflectance parameter, a neutral illuminant (RGB=[1 1 1]) was used. We set the reflectance parameter separately for the R, G and B channel and for the three channels together, in a similar way as we did for the bit values. We took 29 measures per channel, and 29 for their combined activity, for a total of 116.

We used these measures to 1) model the relationship between the input intensity (or reflectance) and the measured luminance, 2) check for additivity, i.e. whether the light emitted by a combination of the three channels is equal to the sum of the lights emitted by each channel activated in isolation, and 3) check whether the relative spectrum emitted by each channel is independent of its level of excitation (channel constancy).

A. Equipment

We use A HTC Vive Pro Eye . This HMD contains two OLED screens (1440 x 1600 pixels each) offering a 110 degree field of view. The refresh rate is 90 frames per second. The computer running the application was using an Intel Core I7-7700K with a 4.20GHz processor and a Nvidia GeForce RTX 2080-Ti graphics card. The Vive Pro was controlled, in turn, using the Unreal Engine 4.22 (18) and the Psychtoolbox 3 (17). We used a Konika Minolta CS2000 tele-spectroradiometer to spectrally characterize the HMD.

of the scenes might affect the color and luminance signal in a complex way, undermining the calibration process.

III. HMD CONTROLLED VIA PSYCHTOOLBOX

A. Relationship between input intensity and luminance

Figure 1 shows the relationship between input bit values and luminance. Luminance increases with bit value for the R, G, B channels (Figure 1A-C) and for the three channels together (Figure 1D), according to a power function. We model this relationship with a standard gamma function:

$$L=b^\gamma \quad (1)$$

With L being luminance (cd/m^2), b the normalized bit value [0-1] and γ the exponent of the power function. We used the `fminsearch()` MATLAB function to find the best estimate for γ , separately for the R,G and B channel. Estimated values were very close to the standard 2.2: 2.2237, 2.1821, 2.2002, for the R, G and B channel, respectively. The average fitting error was minimal: 0.36 cd/m^2 , 0.58 cd/m^2 , and 0.04 cd/m^2 , for the R, G and B channels, respectively.

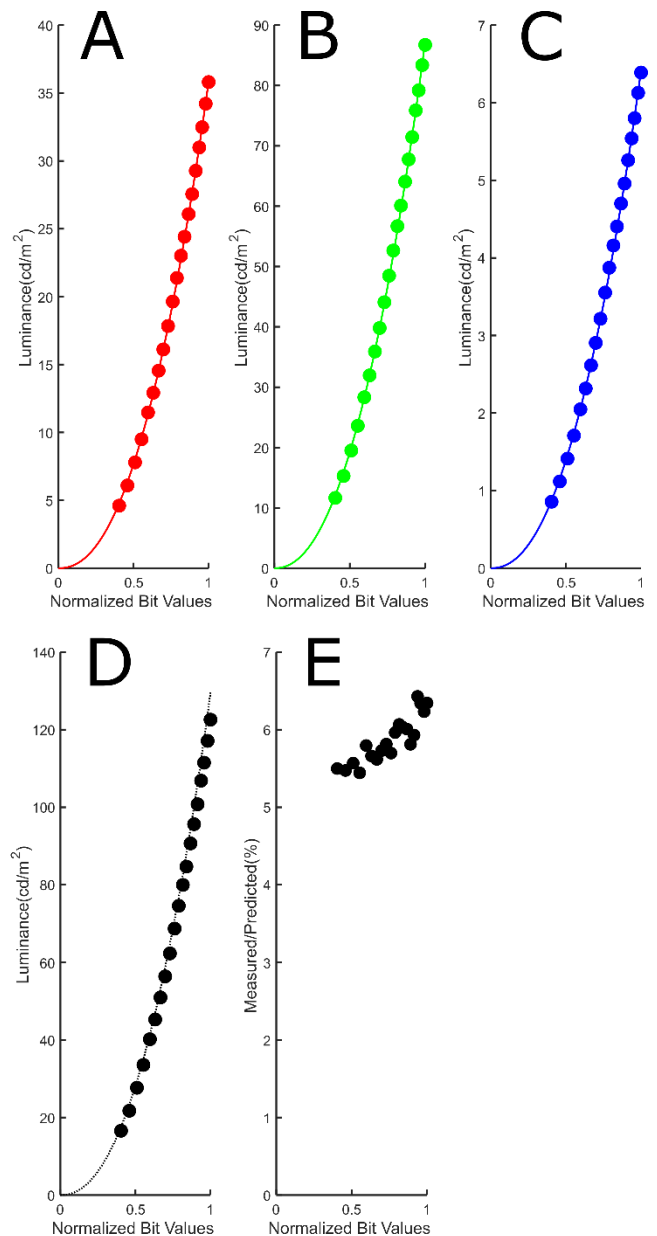


Figure 1. Relationship between input intensity and luminance, HMD controlled via Psychtoolbox. A-D) Normalized bit values on the x-

axis, measured luminance on the y-axis. Red circles for the R channel, green for the G channel and B for the Blue channel. Black data points for the three channels together. In panels A-C, the continuous lines indicate predicted luminance values based on the fitted gamma function. In panel D, the dashed line indicates the predicted luminance based on additivity. E) Additivity check. Normalized bit values on the x-axis, ratio between predicted and measured luminance, on the y-axis, expressed in percentage.

B. Luminance additivity

Figure 1D represents the relationship between luminance and input normalized bit values for the three channels together. The black dots represent the measured luminance, while dashed line refers to the sum of the R,G,B luminance for each bit value. Although the measured luminance is very close to

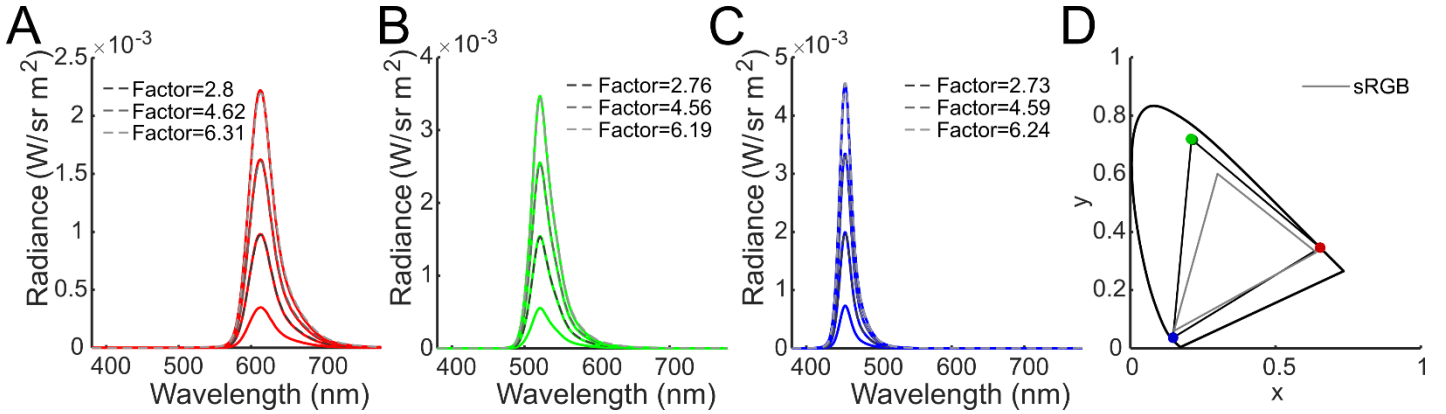


Figure 2. A-C) Measured spectra for the three channels at increasing normalized bit value (~ 0.4, 0.6, 0.8, 1). Wavelength on the x-axis, radiance on the y-axis. In each panel, the four continuous lines represent the measured spectra at the different bit values. The dashed lines represent the predicted spectral profile assuming channel constancy, the legend indicates the multiplicative factor applied to the lowest bit value to predict the other ones. Red lines are for the R channel, green for the G channel and blue for the B channel. D) CIE xy diagram representing the color of the R,G and B channels. The colored points represent the xy chromaticity coordinates of the R,G and B channels. Although all the 20 measures for each channel at different bit value are represented and coded with different intensity (from dark to light) they are almost not visible because their xy coordinates are nearly perfectly overlapping, consistently with channel constancy. The curved black line represents the border of the visible light, the straight black line represents the gamut of the HMD display. The gray line represents the gamut of the sRGB space.

the sum of the R, G and B luminance, the display seems to be slightly sub-additive. Figure 1E confirms this impression: the ratio between the often luminance predicted under the additivity assumption and the measured luminance ranges from 5.4% to 6.4 %.

C. Channel constancy

Figure 2A-C shows the spectra of the three R, G and B channels at different bit values. Increasing the bit value seems to linearly scale the spectral profile, thus leaving the relative spectral profile constant. To test this impression, we estimated the scaling factors for three bit values ([0.6 0.8 1]) and use it to predict the measured spectrum. Predictions (dashed lines) and measured spectral overlap, suggesting near-to-perfect channel constancy. Therefore, the color of each channel should not change with intensity, as visible in Figure 2D, where the color of the R, G and B channels is plotted using colored dots with different intensity coding for different bit values. The dots for each channel are almost completely overlapping, thus indicating the color does not change with the bit value. In Figure 2D also the sRGB gamut is plotted. Remarkably, the gamut we measured is larger than standard sRGB.

D. Calibration test

Overall, the HMD controlled via Psychoolbox seems to fulfill the assumptions for a standard calibration procedure. However, we observed a slight sub-additivity. We tested its impact by presenting on the display 7 colors which are a mixture of R, G and B lights, spanning the center of the xy chromaticity diagram (Figure 3). In order to find the bit values which would allow displaying the selected nominal colors, we applied a standard calibration procedure (15,16). We converted the xy coordinates of each color at a given luminance Y into the corresponding three-stimulus value XYZ. We did the same for the color of the R, G, B channels at maximum luminance, obtaining the matrix M, with R, G and B in rows and XYZ in columns. Then, we computed

linear r,g,b bit values as follows:

$$rgb = M^{-1} \cdot XYZ^T \quad (2)$$

Finally, the linear *rgb* were gamma corrected using the measured gamma functions.

As reported in Figure 3, measured and nominal values are very close, indicating that it is possible to accurately control the color of the emitted light.

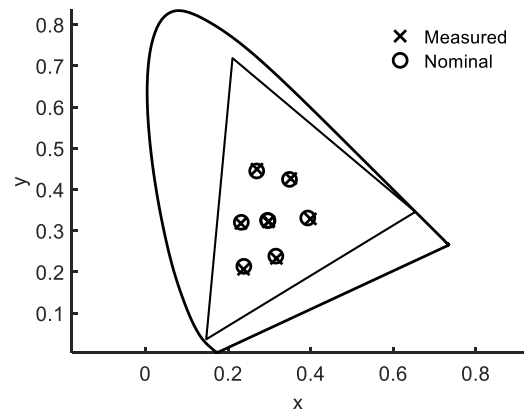


Figure 3. Calibration test. Nominal predicted values (circles) and tested (crosses) values in the xy diagram. The triangle indicates the measured gamut of the HMD.

However, controlling the HMD via Psychtoolbox does not allow to benefit from the possibilities enabled by high resolution rendering systems, typical of modern VR technology. Despite of not allowing a full exploitation of the potentiality of modern VR, arguably this would already represent, for many psychophysical experiments, a better alternative to a standard computer screen, thanks to the large field of view and the lack of the requirement of stabilizing the head. Therefore, we repeated the measures and analyses above while controlling the HMD via the Unreal Engine 4 platform, a suite for real-time rendering which supports VR.

IV. HMD CONTROLLED VIA UNREAL

As mentioned in previous sections, when using the Unreal Engine, we could not directly control the displayed intensity. Instead, we changed the rendering parameters to set the reflectance of a perfectly lambertian surface probe. Such a surface was embedded in a black and white scene (Figure 4), and the virtual camera was set to be directly looking at the circular surface probe (Figure 4B) whose reflectances were systematically varied.

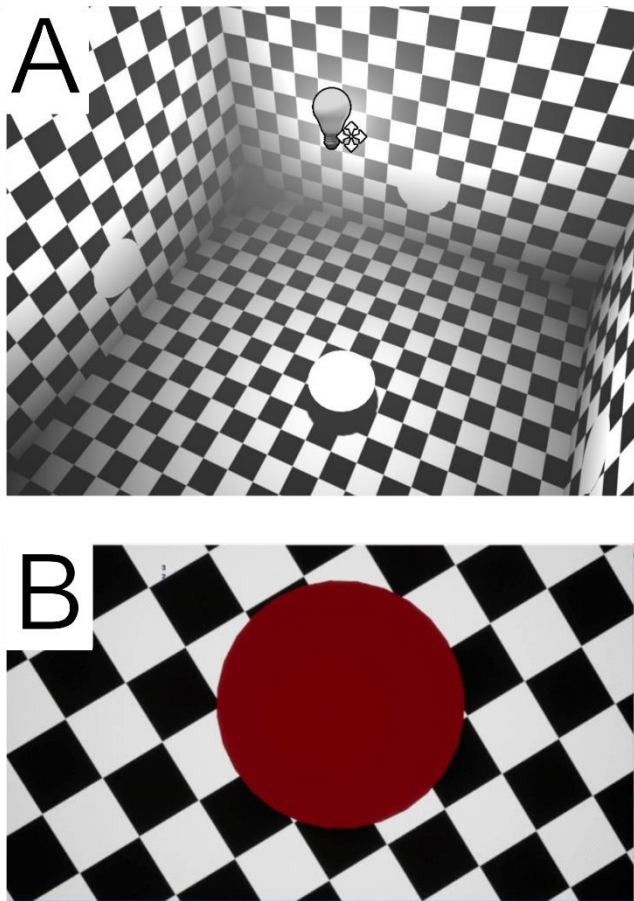


Figure 4. Virtual room and probe surface used for the measures when the HDM was controlled by the Unreal Engine. A) Top view of the room. The checkerboard pattern is composed by white (100% reflectance for the R, G and B channels) to black. The light source position is indicated by the bulb-lamp icon. B) View of the player, as displayed on the HMD.

The room was illuminated by a neutral light source placed above the probe surface (Figure 4A). The distance from the

light source and the probe could be varied to change the illumination intensity.

A. Relationship between input intensity and luminance.

Figure 5 shows the relationship between input reflectance and luminance. Luminance increases with reflectance for the R, G, B channels (Figure 5A-C) and for the three channels together. However, this relationship seems to have a different shape for the R and G channels than for the B channel. Namely, the R and G channels seem to saturate at high reflectance. This might be due to post-processing routines like tone-mapping, not affecting low intensities (as for the B channel).

B. Luminance additivity

Figure 5D represents the relationship between luminance and input reflectance for the three channels together. The black dots represent measured luminance, whereas the dashed line represents the sum of the R, G, B luminance for each reflectance. The display markedly behaves in a sub-additive manner, presumably because of the post-processing routines. Figure 5E shows the ratio between the luminance predicted under the additivity assumption and the measured luminance. The ratio is rather large, reaching up to 40%.

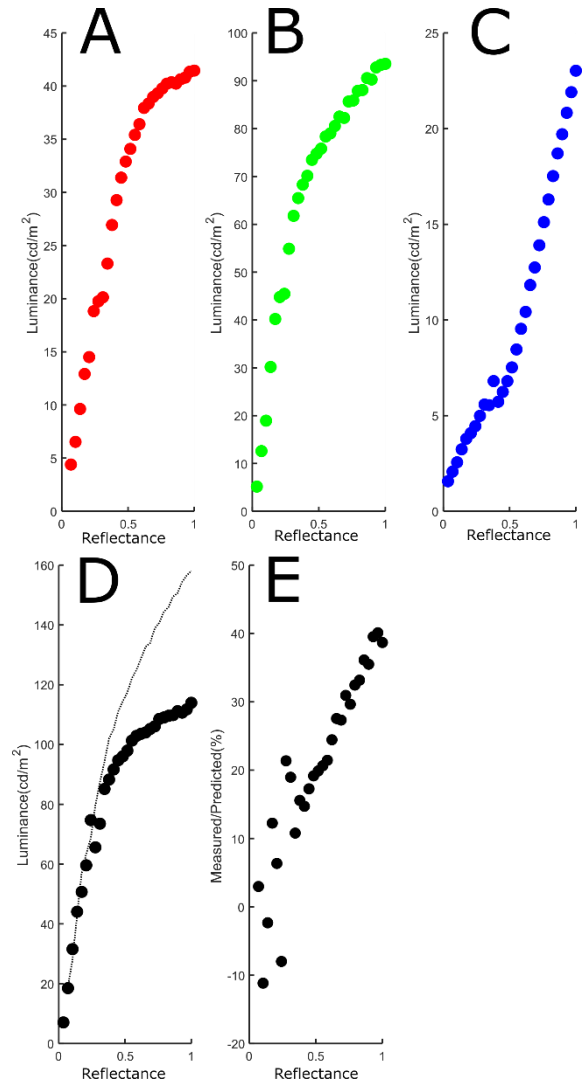


Figure 5. Relationship between input reflectance and luminance, HMD controlled via Unreal Engine, with post-processing routines activated. A-D) Reflectance on the x-axis, measured luminance on

the y-axis. Red circles for the R channel, green for the G channel and B for the Blue channel. Black data points for the three channels together. In panel D, the dashed line indicates the predicted luminance based on additivity. E) Additivity check. Reflectance on the x-axis, ratio between predicted and measured luminance, on the y-axis, expressed in percentage.

C. Channel constancy

Figure 6 A-C shows the spectra of the three R,G and B channels at different reflectance. As opposite to the spectra reported in Figure 2, these spectral profiles present multiple peaks: a main peak similar to the one from the previous measures, and two smaller peaks, as if the three channels were never working in isolation. This could be explained by the typical power management's channel dependency of OLED and AMOLED displays (19). Increasing the reflectance seems to multiplicatively scale the spectral profile. However,

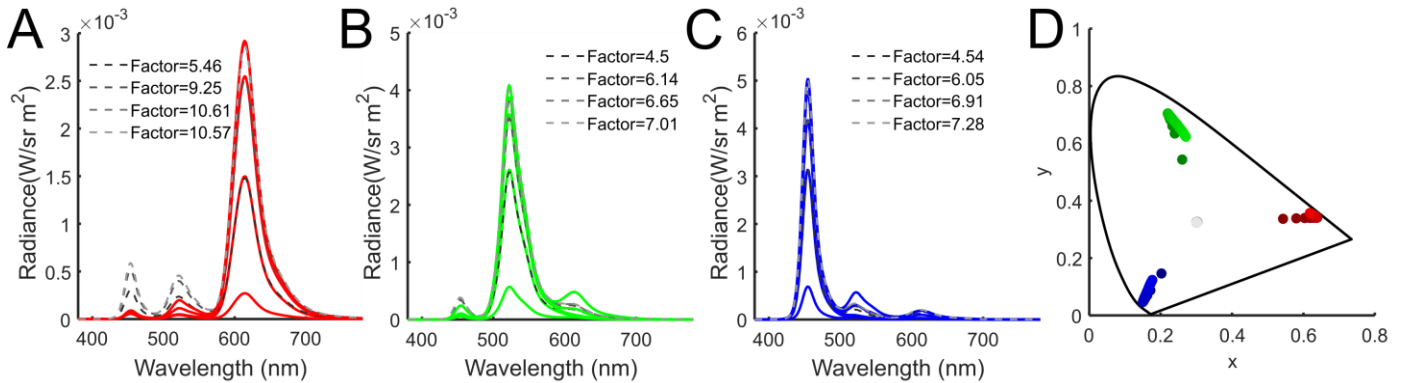


Figure 6 A-C) Measured spectra for the three channels at increasing normalized reflectance ($\sim 0.2, 0.4, 0.6, 0.8, 1$). Wavelength on the x-axis, radiance on the y-axis. In each panel, the four continuous lines represent the measured spectra at the different reflectance. The dashed lines represent the predicted spectral profile assuming channel constancy, the legend indicates the multiplicative factor applied to the lowest reflectance to predict the other ones. Red lines are for the R channel, green for the G channel and blue for the B channel. D) CIE xy diagram representing the color of the R,G and B channels. The colored points represent the xy coordinates of the R,G and B channels. The 29 measures for each channels at different reflectance are represented and coded with different intensity (from dark to light).

as shown by the same analysis described in section III-C, multiplicative scaling cannot explain the behavior of the smaller peaks in the spectral profile. Such a change of the spectral profile with reflectance may explain why the color of the R, G and B channels in terms of their xy coordinates changes with reflectance (Figure 6D).

Therefore, we concluded that controlling the color of the light emitted by the HMD, driven by Unreal Engine cannot be done by means of a standard calibration procedure, without changing the default settings of the engine. The intuition behind is that the non-gamma behavior of the R,G,B channels, the lack of luminance additivity, and the failure of channel constancy were due to the post-processing routines (e.g. tone mapping and auto exposure). Therefore, we repeated the procedure after disabling them.

V. HMD CONTROLLED VIA UNREAL – POST-PROCESSING DISABLED

We repeated the measures and analyses presented in section IV after disabling the following routines in the Unreal Engine: 1) tone mapping was disabled, and 2) the engine scalability settings were set to low quality, except for the view distance tag.

A. Relationship between intensity and luminance

Figure 7 shows the relationship between input reflectance and luminance. The luminance increases with the reflectance for the R, G, B channels (Figure 7A-C) and for the three channels together (Figure 7D), according to a linear function with a clipping point. We model this relationship as follows:

$$L = \begin{cases} s \cdot r, & s \cdot r < p \\ p, & s \cdot r \geq p \end{cases} \quad (3)$$

With L being the luminance (cd/m²), r the input reflectance [0-1] s the slope of the linear function, and p (clipping point) the luminance value after which increasing reflectance does not affect the output. We used the `fminsearch()` MATLAB function to find the best estimate for p and s , separately for the R, G and B channel. The average fitting error was minimal: 0.07 cd/m², 0.15 cd/m², and 0.01 cd/m², for the R, G and B channels, respectively.

B. Luminance additivity

Figure 7D represents the relationship between luminance and input reflectance for the three channels together. The black dots represent measured luminance, the dashed line represents the sum of the R, G, B luminance for each reflectance value. Although measured luminance is very close to the sum of the R, G and B luminance, the display seems slightly sub-additive. The ratio between the luminance predicted under the additivity assumption and the measured luminance ranges from 3.04 to 4.84 % (Figure 7E).

C. Channel constancy

Figure 8A-C shows the spectra of the three R, G and B channels at different bit values. Increasing reflectance seems to multiplicatively scale the spectral profile, thus leaving the relative spectral profile constant. Predictions (dashed lines) and measured spectra overlap, suggesting near-to-perfect channel constancy. The color of each channel does not change much with intensity (Figure 8D). Again, the gamut we measured is larger than the sRGB gamut (Figure 8D).

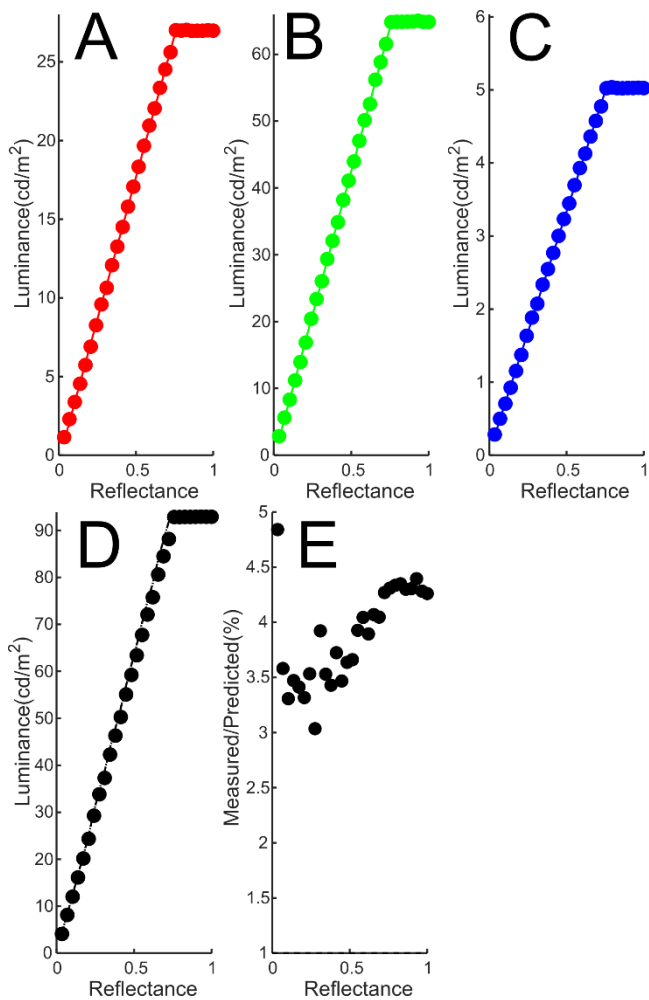


Figure 7. Relationship between input reflectance and luminance, HMD controlled via Unreal Engine with the post-processing routines disabled. A-D) Reflectance on the x-axis, measured luminance on the y-axis. Red circles for the R channel, green for the G channel and B for the Blue channel. Black data points for the three channels together. In panels A-C, the continuous lines indicates predicted luminance values based on the fitted function. In panel D, the dashed line indicates the predicted luminance based on additivity. E) Additivity check. Reflectance on the x-axis, ratio between predicted and measured luminance, on the y-axis, expressed in percentage.

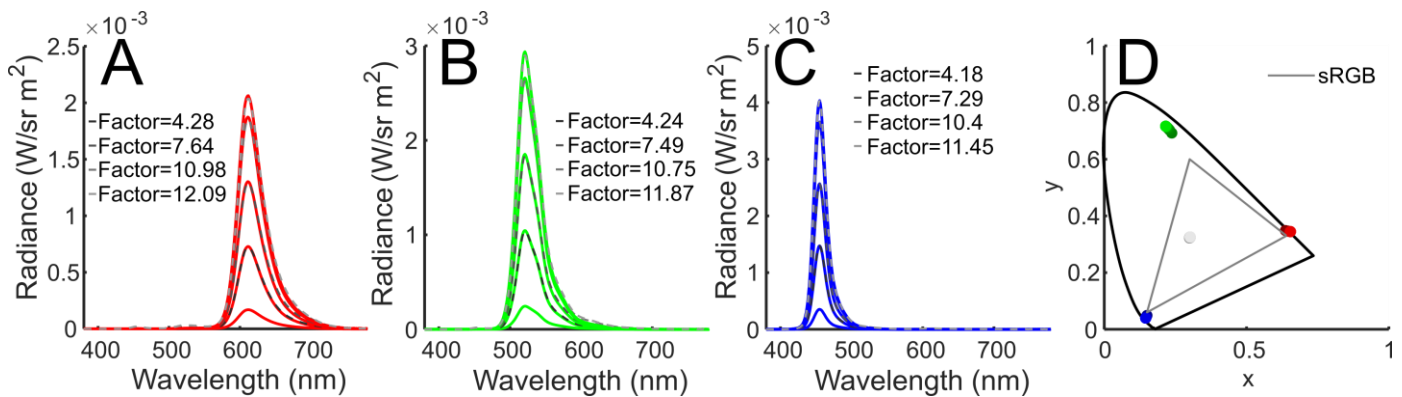


Figure 8 A-C) Measured spectra for the three channels at increasing reflectance ($\sim 0.2, 0.4, 0.6, 0.8, 1$). Wavelength on the x-axis, radiance on the y-axis. In each panel, the four continuous lines represent the measured spectra at the different reflectance. The dashed lines represent the predicted spectral profile assuming channel constancy, the legend indicates the multiplicative factor applied to the lowest reflectance to predict the other ones. Red lines are for the R channel, green for the G channel and blue for the B channel. D) CIE xy diagram representing the color of the R, G and B channels. The colored points represent the xy coordinates of the R, G and B channels. The 29 measures for each channels at different reflectance are represented and coded with different intensity (from dark to light).

D. Calibration test

With the post-processing routines disabled, the HMD seemed to fulfill the assumptions for a standard calibration procedure. Again, we tested its accuracy by presenting on the screen 7 colors which are a mixture of R, G and B lights, spanning the center of the xy chromaticity diagram (Figure 9). In order to find the bit values to produce the chosen nominal color we applied a standard calibration procedure (R). We converted the xy coordinates of each color at a given luminance Y into the corresponding three-stimulus value XYZ. We did the same for the color of the R, G, B channels at maximum luminance, obtaining the matrix M, with R, G and B in rows and XYZ in columns. Then, we computed linear r, g, b bit values according to Eq. 2 and the actual rgb reflectance values using the measured relationship between reflectance and luminance (Eq. 3).

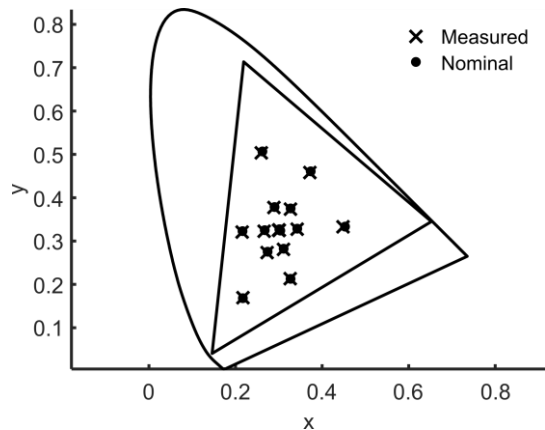


Figure 9. Calibration test. Nominal predicted values (circles) and tested (crosses) values in the xy diagram. The triangle indicates the measured gamut of the HMD

Measured and nominal values are very close, indicating that it is possible to control the color of the emitted light by changing the reflectance values within the Unreal Engine.

We showed that, when controlled via Psychtoolbox, the Vive Pro Eye HMD behaves similarly to a standard computer monitor and therefore a standard calibration procedure is possible. However, the post-processing routines of the Unreal Engine make the problem harder, introducing dependencies between the R, G and B channels (i.e. failure of luminance additivity) and between color and intensity (i.e. failure of channel constancy). After turning off the post-processing routines, a standard calibration procedure allowed to finely control the color of the emitted light depending on the reflectance parameters assigned within the Unreal Engine.

Reflectance does not allow to control the absolute luminance level, which depends on the illumination and viewing conditions. However, we repeated the measures and analyses from section V after increasing the illumination intensity (~50%) by moving the light source closer to the probe surface. We observed that 1) the clipping point p (Eq. 3) did not change, being probably an absolute maximum luminance level for each channel, and 2) the slope s (Eq. 3) of the relationship between reflectance and luminance changed multiplicatively with the same factor for all the channels, i.e. color did not change with changing illumination level. Hence, we are confident that, with the post-processing routines disabled, a standard calibration procedure allows to control the color of matte surfaces in the VR environments rendered with the Unreal Engine.

The color of specular reflection will not directly relate to the rgb input reflectance that we considered in the present work, but on the specific BRDF model used in the rendering process (20). Also, mutual reflections are neglected in the calibration procedure and depend on the rendering algorithm.

In order to overcome the problems posed by the post-processing routines, we simply disable them. Clearly, a much more complicated alternative, would be to characterize and invert the effect of such routines.

Controlling the color of the HMD allows to present observers with realistic stimulation without facing the problems of measuring and real-world stimuli (21-23) or systematically changing the properties of a real scene (6). The Vive Pro Eye HMD incorporates an eye-tracking device, thus, because of the color calibration, the relationship between fixation behavior and color perception can be investigated with richer stimulation than in the past (24-26). To understand how perception operates in real-life, investigators developed realistic goal-directed tasks, such as object recognition based on color (27), or object ranking based on the lightness of their paint (28), or similarity (29,30). With a color calibrated VR setup, the naturalism of such experiments will no longer be limited by presenting the stimuli on a computer monitor, allowing for an immersive experience. With a few exceptions (e.g. 31, peripheral vision has been investigated at limited eccentricity (32-38)). The HMD will allow to precisely control the position of retinal projection, and the color and luminance (via Psychtoolbox) of the stimulation without the need of stabilizing the participants' head or controlling their eye movements, resulting in a more precise experimental control, and in less time consuming and more participants-friendly experimental procedures.

We thank Robert Ennis for his invaluable help with writing the Linux routines to control the HDM via Psychtoolbox. The study was funded by the Deutsche Forschungsgemeinschaft (DFG, German Research Foundation) –project number 222641018 - SFB/TRR135, TPA8 and C2. This work was also supported by the projects MUV App N-250293 and Spectraskin N-288670, both funded by the Research Council of Norway.

REFERENCES

- [1] Bach, M., Meigen, T., & Strasburger, H. (1997). Raster-scan cathode-ray tubes for vision research-limits of resolution in space, time and intensity, and some solutions. *Spatial vision*, 10, 403-414.
- [2] Cowan W. (1995). Displays for vision research. In Bass M. (Ed.), *Handbook of optics, volume 1: Fundamentals, techniques, and design* (pp. 27.1–27.44). New York, NY: McGraw-Hill.
- [3] Overbeck, R. S., Erickson, D., Evangelakos, D., Pharr, M., & Debevec, P. (2018, December). A system for acquiring, processing, and rendering panoramic light field stills for virtual reality. In *SIGGRAPH Asia 2018 Technical Papers* (p. 197). ACM.
- [4] Anthes, C., García-Hernández, R. J., Wiedemann, M., & Kranzlmüller, D. (2016, March). State of the art of virtual reality technology. In *2016 IEEE Aerospace Conference* (pp. 1-19). IEEE.
- [5] Arend, L., & Reeves, A. (1986). Simultaneous color constancy. *JOSA A*, 3(10), 1743-1751.
- [6] Kraft, J. M., & Brainard, D. H. (1999). Mechanisms of color constancy under nearly natural viewing. *Proceedings of the National Academy of Sciences*, 96(1), 307-312.
- [7] Murray, I. J., Daugirdiene, A., Vaitkevicius, H., Kulikowski, J. J., & Stanikunas, R. (2006). Almost complete colour constancy achieved with full-field adaptation. *Vision Research*, 46(19), 3067-3078.
- [8] Fleming, R. W., Dror, R. O., & Adelson, E. H. (2003). Real-world illumination and the perception of surface reflectance properties. *Journal of vision*, 3(5), 347-368.
- [9] Botella, C., Serrano, B., Baños, R. M., & Garcia-Palacios, A. (2015). Virtual reality exposure-based therapy for the treatment of post-traumatic stress disorder: a review of its efficacy, the adequacy of the treatment protocol, and its acceptability. *Neuropsychiatric disease and treatment*, 11, 2533.
- [10] Klinghammer, M., Schütz, I., Blohm, G., & Fiehler, K. (2016). Allocentric information is used for memory-guided reaching in depth: A virtual reality study. *Vision research*, 129, 13-24.
- [11] Fodor, L. A., Coteș, C. D., Cuijpers, P., Szamoskozi, Ș., David, D., & Cristea, I. A. (2018). The effectiveness of virtual reality based interventions for symptoms of anxiety and depression: A meta-analysis. *Scientific reports*, 8(1), 10323.
- [12] Bohil, C. J., Alicea, B., & Biocca, F. A. (2011). Virtual reality in neuroscience research and therapy. *Nature reviews neuroscience*, 12(12), 752.
- [13] Menshikova, G., Bayakovski, Y., Luniakova, E., Pestun, M., & Zakharkin, D. (2013). Virtual reality technology for the visual perception study. In *Transactions on Computational Science XIX* (pp. 107-116). Springer, Berlin, Heidelberg.
- [14] <https://www.sony-depthsensing.com/DepthSense/Markets/HMD>
- [15] Brainard, D. H. (1989). Calibration of a computer controlled color monitor. *Color Research & Application*, 14(1), 23-34.
- [16] Brainard, D. H., Pelli, D. G., & Robson, T. (2002). Display characterization. *Encyclopedia of imaging science and technology*.
- [17] Kleiner M, Brainard D, Pelli D (2007) What's new in Psychtoolbox-3? *Perception* 36:ECVP Abstract Supplement.
- [18] Project website: <http://unrealcv.github.io>
- [19] Kim, C., Hong, S., Lee, K., & Kim, Y. J. (2018). High-Accurate and Fast Power Model Based on Channel Dependency for Mobile AMOLED Displays. *IEEE Access*, 6, 73380-73394.
- [20] Guamera, D., Guamera, G. C., Ghosh, A., Denk, C., & Glencross, M. (2016, May). BRDF representation and acquisition. In *Computer Graphics Forum* (Vol. 35, No. 2, pp. 625-650).
- [21] Giesel, M., & Gegenfurtner, K. R. (2010). Color appearance of real objects varying in material, hue, and shape. *Journal of vision*, 10(9), 10-10.
- [22] Toscani, M., Valsecchi, M., & Gegenfurtner, K. R. (2013). Optimal sampling of visual information for lightness judgments. *Proceedings of the National Academy of Sciences*, 110(27), 11163-11168.

- [23] Granzier, J. J., Brenner, E., & Smeets, J. B. (2009). Reliable identification by color under natural conditions. *Journal of Vision*, 9(1), 1-8.
- [24] Cornelissen, F. W., & Brenner, E. (1995). Simultaneous colour constancy revisited: an analysis of viewing strategies. *Vision Research*, 35(17), 2431-2448.
- [25] Golz, J. (2010). Colour constancy: Influence of viewing behaviour on grey settings. *Perception*, 39(5), 606-619.
- [26] Granzier, J. J., Toscani, M., & Gegenfurtner, K. R. (2012). Role of eye movements in chromatic induction. *JOSA A*, 29(2), A353-A365.
- [27] Radonjić, A., Cottaris, N. P., & Brainard, D. H. (2015). Color constancy in a naturalistic, goal-directed task. *Journal of Vision*, 15(13), 1-21.
- [28] Toscani, M., Valsecchi, M., & Gegenfurtner, K. R. (2017). Lightness perception for matte and glossy complex shapes. *Vision research*, 131, 82-95.
- [29] Guarnera, D., Guarnera, G. C., Toscani, M., Glencross, M., Li, B., Hardeberg, J. Y., & Gegenfurtner, K. (2018). Perceptually validated cross-renderer analytical BRDF parameter remapping. *IEEE Transactions on Visualization and Computer Graphics*. In press. DOI: 10.1109/TVCG.2018.2886877
- [30] Toscani, M., Guarnera, D., Guarnera, G. C. Two perceptual dimensions for specular reflection: gloss and metallic. *Transactions on Applied Perception*, under review.
- [31] Hansen, T., Pracejus, L., & Gegenfurtner, K. R. (2009). Color perception in the intermediate periphery of the visual field. *Journal of Vision*, 9(4), 26-26.
- [32] Weale R. (1953). Spectral sensitivity and wave-length discrimination of the peripheral retina. *The Journal of Physiology*, 119(2-3), 170-90.
- [33] Greenstein, V. C., & Hood, D. C. (1981). Variations in brightness at two retinal locations. *Vision research*, 21(6), 885-891.
- [34] Davis, E. T. (1990). Modeling shifts in perceived spatial frequency between the fovea and the periphery. *JOSA A*, 7(2), 286-296.
- [35] Murray, I. J., Parry, N. R. A., & McKeefry, D. J. (2006). Cone opponency in the near peripheral retina. *Visual neuroscience*, 23(3-4), 503-507.
- [36] Parry, N. R., McKeefry, D. J., & Murray, I. J. (2006). Variant and invariant color perception in the near peripheral retina. *JOSA A*, 23(7), 1586-1597.
- [37] McKeefry, D. J., Murray, I. J., & Parry, N. R. (2007). Perceived shifts in saturation and hue of chromatic stimuli in the near peripheral retina. *JOSA A*, 24(10), 3168-3179.
- [38] Valsecchi, M., Toscani, M., & Gegenfurtner, K. R. (2013). Perceived numerosity is reduced in peripheral vision. *Journal of vision*, 13(13), 1-16.